

# Multimodal Representation Alignment for Cross-modal Information Retrieval

Fan Xu<sup>a</sup>, Luis A. Leiva<sup>a,\*</sup>

<sup>a</sup>*Department of Computer Science, University of Luxembourg, 6, avenue de la Fonte, Esch-sur-Alzette, L-4364, Luxembourg*

---

## Abstract

Different machine learning models can represent the same underlying concept in different ways. This variability is particularly valuable for in-the-wild multimodal retrieval, where the objective is to identify the corresponding representation in one modality given another modality as input. This challenge can be effectively framed as a feature alignment problem. For example, given a sentence encoded by a language model, retrieve the most semantically aligned image based on features produced by an image encoder, or vice versa. In this work, we first investigate the geometric relationships between visual and textual embeddings derived from both vision-language models and combined unimodal models. We then align these representations using four standard similarity metrics as well as two learned ones, implemented via neural networks. Our findings indicate that the Wasserstein distance can serve as an informative measure of the modality gap, while cosine similarity consistently outperforms alternative metrics in feature alignment tasks. Furthermore, we observe that conventional architectures such as multilayer perceptrons are insufficient for capturing the complex interactions between image and text representations. Our study offers novel insights and practical considerations for researchers working in multimodal information retrieval, particularly in real-world, cross-modal applications.

**Keywords:** Multimodal Models, Embedding Spaces, Feature Alignment, Contrastive Loss, Learning to Rank, Zero-shot Performance

---



---

\*Corresponding author.

*Email addresses:* fan.xu@uni.lu (Fan Xu), luis.leiva@uni.lu (Luis A. Leiva)

*URL:* 0009-0008-6246-267X (Fan Xu), 0000-0002-5011-1847 (Luis A. Leiva)

## 1. Introduction

Multimodal Machine Learning (MML) has made huge progress thanks to recent advancements in vision and language models. The Convolutional Neural Network (CNN) architecture [1] has been one of the most outstanding models in Computer Vision, nowadays superseded by the Transformer architecture [2], in particular the Vision Transformer architecture (ViT) [3] when training on very large datasets. In Natural Language Processing, we can find various Large Language Models (LLMs) such as BERT [4] or the Generative Pre-trained Transformers (GPT) [5, 6, 7], which offer new possibilities for constructing MML models.

Within the plethora of MML models, Vision-Language Models (VLMs) are increasingly being adopted in downstream tasks, including Information Retrieval (IR), Visual Question Answering (VQA), and image captioning, among others. For example, CLIP [8] utilizes an image encoder and a text encoder to contrast representations from images and texts, achieving competitive zero-shot classification performance. BLIP [9] builds upon the idea of CLIP and uses the Transformer architecture with a triple loss objective, achieving state-of-the-art (SOTA) performance in some downstream tasks. The core of the success of VLMs is attributed to the fact that they create representations in a shared embedding space that accounts for vision and language modalities jointly. These models have an enormous potential for in-the-wild multimodal IR, i.e., finding the corresponding representations of one modality given another modality as inputs. This can be framed as a feature alignment task. For example, given the semantics in a sentence that is encoded by a language model such as BERT, find the closest image that conveys the same textual semantics but based on the representations provided by an image encoder such as ViT, or vice versa. Inspecting whether aligned features relate to the embedding geometry is of particular importance, as well-aligned representations usually enhance downstream task performance [10]. However, it remains unclear whether this improvement is also reflected by the geometry of the embedding spaces, especially when compared to unaligned spaces. Unfortunately, little is known about these phenomena in VLMs and their connection to downstream tasks.

To bridge this gap in the research literature, we first analyze the latent spaces created by three SOTA VLMs and three unimodal models combined (i.e., the combination of three vision models with three language models). Next, we investigate standard metrics to measure cross-modality similar-

ity (Euclidean, Manhattan, and Chi-square distances, and cosine similarity) as well as learned metrics (Mean Squared Error and a custom contrastive loss) to align vision and language representations extracted by the aforementioned multimodal and combined unimodal models. We found that, when using CLIP or BLIP representations, cosine similarity outperforms the learned metrics by a significant margin. We also found that aligning representations from combined unimodal models via Multi-layer Perceptrons (MLPs) does not succeed at cross-modal downstream IR tasks. We conclude therefore that feature alignment performs best with MML models that are trained from scratch with contrastive loss. Taken together, this paper makes the following contributions:

- An exploration of the embedding spaces created by multimodal and combinations of unimodal models, from which we find that BLIP achieves the minimal modality gap across evaluated models, while a distribution distance like  $W_2$  can also quantify this.
- A systematic examination of several metrics for measuring cross-modal embedding similarity, including standard and custom (learned) ones, for which we find that cosine similarity outperforms among other metrics.
- An experimental verification of the incapability of MLPs to learn similarity scores from high-level representations (even though the Universal Approximation Theorem [11] states it is possible), indicating a discrepancy between theory and practice.
- A series of systematic retrieval experiments using text queries to retrieve images, and vice versa.

## 2. Related Work

MML models are typically constructed upon unimodal models, each of which is designed to process a single modality—such as images, audio, text, or time series data. For the sake of simplicity, this work focuses specifically on VLMs. Accordingly, we begin by reviewing foundational models in the vision and language domains, followed by an overview of prominent VLMs. We then examine contrastive learning methods and their application to multimodal IR tasks.

### *2.1. Vision Foundation Models*

CNN architectures are foundational in the field of computer vision [12], serving as a cornerstone of deep learning for a wide range of vision tasks. Among these, ResNet [13] remains a widely adopted architecture due to its robust performance and versatility. More recently, ViT-based models have gained popularity, owing to their inherent parallelization and scalability advantages. Notable examples include ConViT [14] for image classification and ViTDet [15] for object detection. Concurrently, efforts have been made to enhance CNN performance through architectural innovations. For instance, ConvNeXt [16], which retains a purely convolutional structure, has demonstrated superior performance over the hierarchical Swin Transformer [17] on both object detection and segmentation benchmarks.

Despite the strong performance of modern vision models across a range of tasks, a systematic investigation into the relationship between embedding spaces and downstream task performance remains limited. In this work, we address this gap by analyzing the embedding spaces of diverse vision and language models.

### *2.2. Language Foundation Models*

The Transformer architecture serves as the foundational backbone for all modern LLMs. Built upon this framework, BERT [4] introduced deep bidirectional representations learned from unlabeled text; RoBERTa [18] significantly enhanced BERT’s performance through more robust training strategies; and DeBERTa [19] further improved pre-training efficiency via a disentangled attention mechanism and an enhanced mask decoder. Taking a different approach, XLNet [20] employed a permutation-based language modeling objective to unify the strengths of both autoregressive and autoencoding methods. The GPT family has also seen consistent progress. GPT-1 [5] introduced a single task-agnostic model using generative pre-training followed by discriminative fine-tuning. GPT-2 [6] demonstrated that large-scale language models can acquire a wide range of capabilities without task-specific supervision. GPT-3 [7] showed that scaling model size yields significant gains in zero-shot, one-shot, and few-shot performance, sometimes rivaling fine-tuned models. Other SOTA LLMs include LLaMA [21], which surpasses GPT-3 in performance despite being an order of magnitude smaller; BLOOM [22], which achieves strong results via multi-task fine-tuning; and GLM [23], which outperforms both BERT and GPT-style models in various benchmarks.

When combined with vision models, these LLMs allow for a more nuanced exploration of the geometry of multimodal embedding spaces. This enables comparison between jointly trained VLMs and those trained separately, offering insights into cross-modal representation learning.

### 2.3. Vision-Language Models

The proliferation of vision and language models has significantly expanded opportunities for developing novel VLMs. Among these, CLIP [8] represents a widely adopted framework, leveraging contrastive loss as its primary training objective. Building upon this paradigm, BLIP [9] extends functionality beyond image classification to VQA and retrieval tasks, while BLIP-2 [24] advances efficiency by integrating a frozen image encoder with a language model to bootstrap vision-language pretraining. Concurrently, alternative architectures have emerged: Meta-Transformer [25] introduces a unified framework for multimodal learning, encoding up to 12 modalities within a shared embedding space without paired data. Similarly, CoDi [26] enables parallel generation of arbitrary output combinations from diverse input modalities through feature alignment in diffusion models. Further contributions from VLMs [27, 28, 29, 30, 31] and multimodal LLMs [32, 33, 34, 35] continue to enrich the architectural diversity and training methodologies within MML.

However, prior research lacks a systematic comparative analysis of embedding spaces across diverse VLMs. To address this gap, we empirically investigate embedding structures using three MML models, contrasting them with unimodal baselines.

### 2.4. Contrastive Learning

The success of VLMs hinges on contrastive learning [36], a paradigm initially developed to learn invariant mappings in single-modality datasets. Early contrastive methods like [37] paired data points using prior knowledge (e.g., class labels) and measured similarity via Euclidean distance between representations in a "vanilla" contrastive loss framework.

This foundation evolved with CPC [38], which introduced InfoNCE, a contrastive loss based on unnormalized cross-entropy using cosine similarity. InfoNCE maximizes mutual information between latent representations by treating the task as a classification problem over positive and negative pairs. Building on this, MoCo [39] proposed a momentum-based framework:

a query encoder is trained via backpropagation, while a key encoder is updated via exponential moving averages (EMA). MoCo maintains a dynamic queue of encoded keys from previous batches, enabling efficient sampling of negatives for InfoNCE. Crucially, gradients only update the query encoder, decoupling training stability from batch size. SimCLR [40] further simplified contrastive learning by relying solely on in-batch negatives. It replaced Euclidean distance with cosine similarity in a normalized, temperature-scaled InfoNCE loss, emphasizing the importance of strong data augmentations. Unlike MoCo, SimCLR requires large batches to sample sufficient negatives but achieves competitive performance with minimal architectural complexity. Diverging from explicit negative sampling, BYOL [41] introduced a bootstrapping approach. An online network learns to predict the output of a slowly evolving target network (updated via EMA) using mean squared error. By eliminating negative pairs entirely, BYOL avoids collapse through asymmetric architectures and momentum updates, demonstrating that contrastive learning can thrive without explicit negatives.

To bridge vision and language modalities, models like CLIP and ALIGN [42] extended contrastive learning to multimodal data. Both employ InfoNCE with softmax-normalized cosine similarity to align image-text pairs, but differ in scale and data strategy. CLIP uses curated datasets, while ALIGN leverages larger noisy web-scale datasets. Beyond softmax-based losses, SigLIP [43] introduced a sigmoid loss for image-text contrastive learning using cosine similarity. This approach replaces pairwise softmax normalization with element-wise sigmoid, enabling symmetry between image-to-text and text-to-image tasks. SigLIP reduces memory overhead by avoiding batch-wise dependencies, achieving efficiency without sacrificing performance.

Nevertheless, contrastive learning promotes a modality gap, causing a narrow cone effect where all representations reside in a small region of high-dimensional spaces, as evidenced by Liang et al. [10]. Their work demonstrates that this modality gap substantially impacts downstream performance and is modulated by the loss function’s temperature parameter, concluding that an optimal gap magnitude varies across tasks, benefiting some while hindering others. Corroborating this, research in recommender systems [44] associated a reduced modality gap with enhanced downstream performance. Ethayarajh [45] also noted that word embeddings from LLMs are highly anisotropic using self-similarity and intra-sentence similarity metrics, indicating a positive cosine similarity even when they are semantically different.

In contrast to prior work, we study neural networks with a custom con-

trastive loss function to directly learn similarity metrics between representations, thereby investigating the viability and efficacy of this approach.

### 2.5. Applications in Information Retrieval

VLMs facilitate cross-modal IR through similarity-based metrics, proving particularly advantageous for real-world IR applications. Specifically, backbone encoders from multimodal architectures can extract feature representations from disparate datasets, subsequently identifying latent semantic commonalities via representation alignment. This process involves, for any given representation in one modality, ranking candidate representations across other modalities using a (dis)similarity metric and returning the top- $K$  matches.

Beyond direct utilization of multimodal models for aligned-representation retrieval, several methodologies enhance cross-modal alignment. Wang et al. [46] developed mapping functions to project diverse modalities into a unified embedding space, conceptually analogous to Meta-Transformer frameworks. Luo et al. [47] introduced a multi-task learning approach for image-text retrieval that demonstrates empirical superiority over competing methods. Additionally, Zhen et al. [48] employed transfer learning with modality-specific neural networks to optimize cross-modal retrieval performance. In e-commerce domains, Kumar et al. [49] leveraged contrastive loss within unimodal models to learn discriminative representations, retrieving top- $K$  similar products through approximate nearest-neighbor search. Notably, Luo et al. [50] aggregated hierarchical features from diffusion model U-nets to establish semantic correspondences across images. Concurrently, Beltrán et al. [51] adapted VQA architectures to fuse visual-textual representations for enhanced search capabilities, while Yu et al. [52] addressed the modality gap [10] via structured attention networks for language-to-vision retrieval.

Despite these methodological advances, the relationship between structural properties of multimodal embedding spaces and retrieval efficacy remains inadequately characterized in the existing literature.

## 3. Methodology

We are interested in aligning learned feature representations (embeddings) in different modalities coming from vision models, language models, or VLMs. Let  $\mathcal{D} = \{(\mathbf{x}_i, \mathbf{y}_i), i = 1, \dots, N\}$  be a dataset that contains  $N$  paired samples consisting of text  $\mathbf{x}_i$  and corresponding image  $\mathbf{y}_i$ . Let  $f(\cdot)$  and  $g(\cdot)$

be text and image encoders, respectively, which can either be multimodal or unimodal models. The extracted text representations  $\hat{\mathbf{x}}_i = f(\mathbf{x}_i) \in \mathbf{P}$  and image representations  $\hat{\mathbf{y}}_i = g(\mathbf{y}_i) \in \mathbf{Q}$  are mapped into a common Euclidean embedding space, where  $\mathbf{P} \subset \mathbb{R}^n$  is the text feature space and  $\mathbf{Q} \subset \mathbb{R}^n$  is the image feature space.

After extracting features by these models, we maps all features to a 2D space using various dimensionality reduction methods (we tested t-SNE [53] and UMAP [54]), and then investigate the geometric structure of embedding spaces and their connection to the performance of retrieval tasks.

To measure the similarity between two representations, we can apply multiple metrics to obtain  $d(\hat{\mathbf{x}}_i, \hat{\mathbf{y}}_i)$ , where  $d(\cdot, \cdot)$  is a (dis)similarity function. We first use 4 standard metrics (Euclidean, Manhattan, and Chi-Square distance, and cosine similarity; see Table 1) that can measure how close (or different) are two representations  $\hat{\mathbf{x}}_i \in \mathbb{R}^n$  and  $\hat{\mathbf{y}}_i \in \mathbb{R}^n$ , motivated by previous work [55, 56, 57, 58]. We should note that cosine similarity is in the range of  $[-1, 1]$ , while the dissimilarity metrics are unbounded. We then find the corresponding representations between modalities by ranking the values according to each metric and retain the top- $K$  matches. In other words, for each representation in one modality, we compute its similarity against all the representations in the other modality in a dataset and retrieve the top ranked similarity scores. We follow this process in both text-to-image and image-to-text experiments (Section 4.5).

**Table 1:** Standard metrics concerned.  $\mathbf{p} \in \mathbb{R}^n$  and  $\mathbf{q} \in \mathbb{R}^n$  are feature representations and  $d(\cdot, \cdot)$  is the (dis)similarity between them.

Euclidean distance	$d(\mathbf{p}, \mathbf{q}) = \sqrt{\sum_{i=1}^n (p_i - q_i)^2}$
Cosine similarity	$d(\mathbf{p}, \mathbf{q}) = \frac{\sum_{i=1}^n p_i q_i}{\sqrt{\sum_{i=1}^n p_i^2} \sqrt{\sum_{i=1}^n q_i^2}}$
Manhattan distance	$d(\mathbf{p}, \mathbf{q}) = \sum_{i=1}^n  p_i - q_i $
Chi-square distance	$d(\mathbf{p}, \mathbf{q}) = \frac{1}{2} \sum_{i=1}^n \frac{(p_i - q_i)^2}{p_i + q_i}$

As a step forward, we learn to align representations extracted by different



models using an MLP  $Z(\cdot)$  with best architectures searched by Optuna,<sup>1</sup> ranging from 1 to 5 layers with a number of neurons from 100 to 1100. The MLP with ReLU activation function in hidden layers takes as inputs concatenated text and image representations and outputs a single scalar in range  $[-1, 1]$  through  $\tanh$  activation function at the final layer, akin to the cosine similarity, since it has been used as a loss term in previous MMLs such as CLIP and BLIP.<sup>2</sup> We first use the Mean Squared Error (MSE) as the loss function to learn cosine similarity via MLPs, as MSE is simple yet powerful in regression tasks. We also propose a more specific contrastive loss [37] as the objective of MLPs to learn from representations, with the goal of pulling similar features together (towards value 1) while pushing dissimilar features apart (towards value -1), as shown in Equation 1:

$$\mathcal{L}(\hat{\mathbf{x}}_i, \hat{\mathbf{y}}_j) = I_{ij} \frac{1}{2} (1 - \hat{d}_{ij})^2 + (1 - I_{ij}) \frac{1}{2} [\hat{d}_{ij} + 1]^2 \quad (1)$$

where  $\hat{d}_{ij} = Z(\text{cat}(\hat{\mathbf{x}}_i, \hat{\mathbf{y}}_j))$  is the output of the MLP that takes concatenated representations from images and texts as inputs, and  $I_{ij}$  is the indicator function shown in Equation 2:

$$I_{ij} = \begin{cases} 1, & i = j \\ 0, & i \neq j \end{cases}. \quad (2)$$

Averaging over the loss  $\mathcal{L}(\hat{\mathbf{x}}_i, \hat{\mathbf{y}}_j)$  of all image representations  $\hat{\mathbf{y}}_j$  in the dataset against a given text representation  $\hat{\mathbf{x}}_i$ , we get the loss for a text representation. Concretely, the loss of a text representation  $\hat{\mathbf{x}}_i$  with regard to all image representations  $\hat{\mathbf{y}}_j, j = 1, \dots, N$  is:

$$\mathcal{L}(\hat{\mathbf{x}}_i) = \frac{1}{N} \sum_{j=1}^N \mathcal{L}(\hat{\mathbf{x}}_i, \hat{\mathbf{y}}_j), \quad (3)$$

where  $N$  is the total number of samples in the dataset. The same holds for the loss  $\mathcal{L}(\hat{\mathbf{y}}_i)$  of an image representation  $\hat{\mathbf{y}}_i$  against all text representations  $\hat{\mathbf{x}}_i, i = 1, \dots, N$  in the same dataset. The final objective over all data samples is:

$$\mathcal{L}(\mathcal{D}) = \frac{1}{N} \sum_{i=1}^N \mathcal{L}(\hat{\mathbf{x}}_i) = \frac{1}{N} \sum_{j=1}^N \mathcal{L}(\hat{\mathbf{y}}_j). \quad (4)$$

---

<sup>1</sup><https://optuna.org/>

<sup>2</sup>Although CLIP and BLIP convert similarity scores to probabilities.

The MLP is trained with Adam optimizer ( $\beta_1 = 0.9, \beta_2 = 0.999$ ) with a scheduled learning rate of  $5 \cdot 10^{-5}$  up to 100 epochs with a decay  $(1 + 2^{0.5c})^{-1}$ , where  $c$  is the current epoch.<sup>3</sup> We use a batch size of 64 and Early Stopping: training stops if the validation loss does not improve over 1% compared to that of the previous epoch for 5 consecutive epochs, and the best model weights are retained.

#### 4. Experiments

Figure 1 illustrates our comprehensive experimental pipeline. Initially, we employ both multimodal and unimodal architectures as feature extractors to derive representations from three distinct datasets. Subsequently, we examine the relationship between retrieval performance and the geometric structures of these representations. We quantitatively evaluate cross-modal retrieval efficacy using the aforementioned metrics, assessing both image and text representations. Following this analysis, we train neural network models on the extracted representations and validate their performance on retrieval tasks. Finally, we present real-world retrieval experiments to provide further validation.

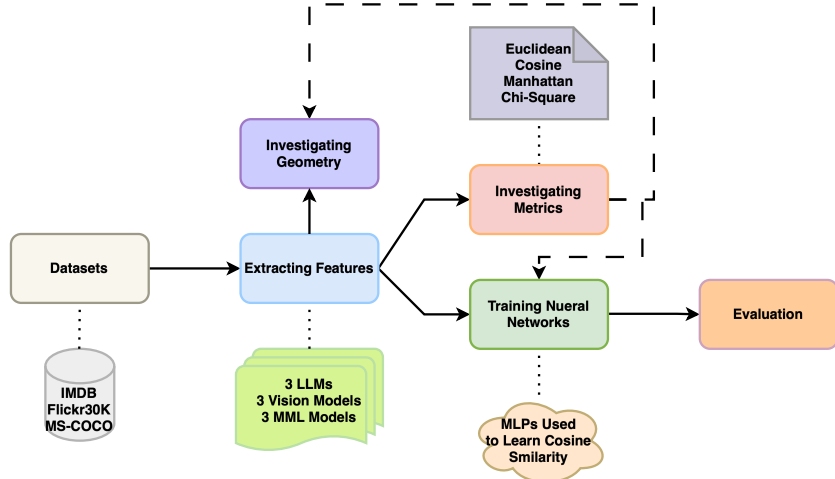


Figure 1: Pipeline of our experiments.

<sup>3</sup>This decay proved useful in preliminary experiments.

#### 4.1. Datasets

We use three public benchmarks: the “IMDB Vision and NLP” dataset [59], which contains 4K movie posters with corresponding names, Flickr30K [60], having 31K images and 155K comments, and MS-COCO [61] (Train2017 subset), with 118K images and 590K captions. All datasets are complementary and of different nature, from which models’ capability of understanding visually different scenarios can be thoroughly tested. IMDB mainly focuses on visual impression of movie posters, Flickr30K contains images showing complex interactions between people and objects, and MS-COCO emphasizes multiple objects in context. To simplify the problem, we assume a one-to-one mapping between modalities, i.e., one textual description can have only one ground-truth image, and vice versa. Since Flickr30K and MS-COCO have 5 text descriptions (comments or captions) associated with each image, we choose the first description for our experiments. We resize all images to the same size of  $224 \times 224$  px and normalize each pixel value in the range  $[0, 1]$ , as usual in vision models. Note that resizing images to  $224 \times 224$  px does not necessarily hinder model’s visual understanding capability, as evidenced by Bica et al. [62], from which images were resized to  $224 \times 224$  px while still capturing fine-grained details in images.

#### 4.2. Models

As mentioned previously, we focus on vision and language modalities, and therefore we combine separated vision models with language models or use already existing VLMs. Out of the plethora of SOTA models, and based on their official naming routines, we use three VLMs: CLIP-ViT-B/32 (CLIP for short), BLIP-base-retrieval-CoCo (BLIP), Meta-Transformer-B/16 (Meta-Transformer), and three composed models by combining vision with language models: ResNet-34 with BERT-small (denoted as ResNet/BERT), ConViT-base with RoBERTa-base (ConViT/RoBERTa), as well as ConvNeXt-small-1K with XLNet-base-cased (ConvNeXt/XLNet). We extract representations from the layer before the final output layer from each model, which are deemed as learned feature representations.

Vision and language features have compatible dimensions if they are extracted by any of the 3 multimodal models. This is natural for multimodal models, as they output features with same dimension. However, we intentionally select uni-modal models so that composed models can have compatible image and text features. Moreover, the feature dimensions might be different when using different model as well (e.g., features extracted by CLIP have 512

dimensions while features extracted by BLIP have 256 dimensions), which will not impact the training of MLPs, as their input sizes fit the sizes of concatenated features as inputs. For later analyses in [Section 4.3](#) to [Section 4.5](#), all the experiments are conducted on features extracted by either multimodal models or combined unimodal models as mentioned in this section.

#### 4.3. Embedding Space Analysis

We first project the extracted features for each model and dataset into a 2D space for intuitive visualization. We use the non-linear projection algorithm t-SNE, given that linear alternatives such as Principal Component Analysis [63] (PCA) do not capture well the complex structure of embedding spaces. UMAP [54] also fails to preserve the geometric structure of these spaces when we plot the embedding spaces. To ease visualization, the plots in [Figure 2](#) use a random selection of 2K data samples from each dataset, to avoid showing over-dense and overlapped clusters. Dashed lines denote the cluster contours, computed by a Support Vector Machine (SVM) [64] with a Gaussian kernel. Yellow dots in [Figure 2](#) denote the centroids of each modality cluster. The modality gap is computed via Euclidean distance between centroids in the original dimension (instead of the reduced dimension by t-SNE), as defined in [10], shown on the top-right corner of each subplot.

**Table 2:** Wasserstein-2 distance ( $\downarrow$ ) between image representations and text representations in the original dimension. Best results are highlighted.

	CLIP	BLIP	Meta	UM1	UM2	UM3
<b>IMDB</b>	60.74	42.72	125.12	528.40	114.83	11668.23
<b>Flickr30K</b>	56.40	43.18	80.52	524.39	99.20	8186.30
<b>MS-COCO</b>	60.41	41.89	75.68	525.61	102.50	6916.52

In IMDB (first row of [Figure 2](#)) we can see that BLIP promotes the shortest modality gap over 3 multimodal models, followed by CLIP. Interestingly, we also observe that even unaligned embeddings of ConViT/RoBERTa and Meta-Transformer have small modality gaps, except for ConvNeXt/XLNET. Notably, we observe a large cluster contour separation in Meta-Transformer among multimodal models, while the combined unimodal models have similar contour separation.

In Flickr30K (second row of [Figure 2](#)) the modality gaps for all multimodal models are quite similar, even though BLIP turns out to be the

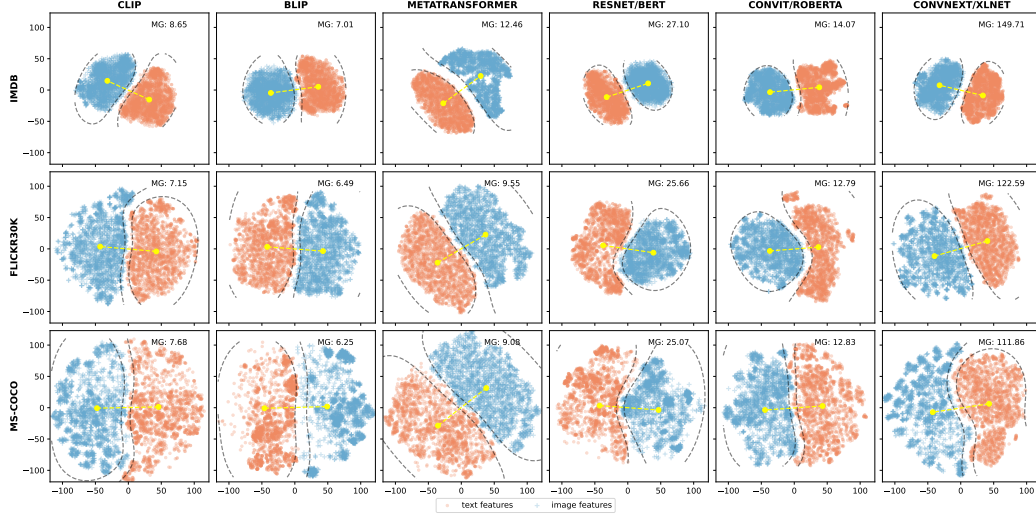


**Figure 2:** Embedding spaces of multimodal models and combined unimodal models on different datasets through t-SNE. **Image features** are in blue while **text features** are in orange. Dashed lines (--) denote cluster contours, and yellow dots (●) denote centroids of clusters, for which the modality gap (MG) is shown on the top-right part of each plot.

smallest one. No significant differences between cluster contours were observed. Among all combined unimodal models, ConViT/RoBERTa promotes the shortest modality gap, and all combined unimodal models have larger modality gaps than those of any multimodal models.

In MS-COCO (third row of Figure 2), BLIP has the smallest modality gap among all multimodal models, despite that the difference is small overall. Again, the modality gaps of all unimodal models are much larger than those of multimodal models. Cluster contours do not exhibit large differences either.

From all plots, the Euclidean distance, used by previous work to measure the modality gap, reflects the effects of alignment between varying modalities. Besides measuring the modality gap between centroids of representation clusters, we also compute in Table 2 the Wasserstein-2 distance (namely a distribution distance) to measure the cost of transport data points from one distribution to another distribution.<sup>4</sup> Note that Wasserstein distance is sym-

<sup>4</sup>To compute the Wasserstein-2 distance, we randomly split each dataset to 5K batches and average the running distance over all batches to avoid memory issues.

metric to two input representations.

We use the following shorthands for **all** related tables: Meta for Meta-transformer, UM1 for ResNet/BERT, UM2 for ConViT/RoBERTa, and UM3 for ConvNeXt/XLNet. From [Table 2](#), we observe the same trend as that of using Euclidean distance to measure the modality gap. Concretely, we find that BLIP consistently has the smallest modality gap among other models, which serves as an inspiration to align representation distributions between two modalities instead of fixed representation extracted by each encoder. However, models with smaller modality gap do not necessarily show better performance than other models, as evidenced by the results in [Section 4.5](#). For example, although Meta-Transformer shows a closer modality gap among other models to these of CLIP and BLIP, the performance is almost the same as other combined uni-modal models overall.

We noted an interesting trend, however: embedding distributions tend to be sparser as dataset size increases, regardless of the model. Overall, we can conclude that (1) the alignment among different modalities can be measured neither by spatial distances (e.g., Euclidean) nor by distribution differences (e.g., Wasserstein distance); and (2) well-aligned representations of CLIP and BLIP and unaligned representations of other models do not show much distinctive geometry for the same dataset.

#### 4.4. Feature Similarity Analysis

To corroborate the effect of feature alignment in multimodal models and combined unimodal models, [Figure 3](#) shows the cosine similarity matrices of 10 randomly selected <text,image> pairs (for visualization purposes) from each dataset using different models. We can see that text features and corresponding image features are well aligned by CLIP and BLIP, as indicated by the diagonal, which is the consequence of harnessing contrastive loss as the whole or a part of the training objectives. In addition, cosine similarity from multimodal models has a higher maximum than combined unimodal models overall, which suggests that the feature alignment from multimodal models somehow improves the similarity between embeddings. Note that Meta-Transformer has consistently yields cosine similarity more than 0.9 for any text-image pairs, which indicates that all representations are clustered in a small region of high dimensional spaces (its original dimension is 768 while [Figure 2](#) shows 2D representations reduced by t-SNE). This phenomenon imposes challenges when applying it to downstream tasks, as all representations are deemed as highly similar across modalities. Although

retrieval task is done by ranking similarity scores (cosine similarity in this case), the retrieved results will not be much distinguished from each other. Meta-Transformer is not trained with paired text-image data, so it is not surprising that it cannot pull together similar representations or push apart dissimilar ones.

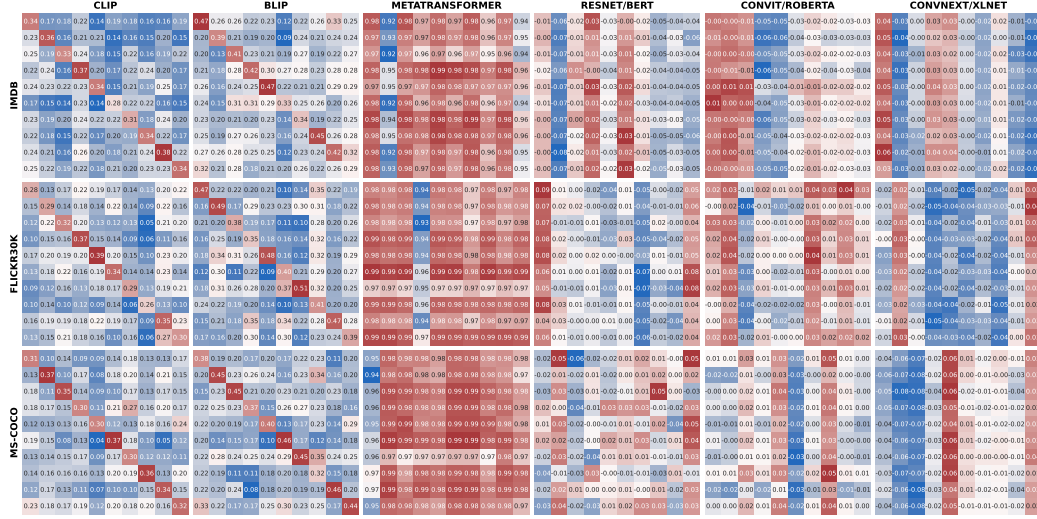


**Figure 3:** Cosine similarity ( $\uparrow$ ) matrix of a random selection of 10  $\langle \text{text}, \text{image} \rangle$  pairs. In each cell, cosine similarity is computed based on text and image features from the dataset showed on the left, extracted by models listed on the top. In each heatmap, the X-axis denotes text features and the Y-axis denotes the image features. Red cells have **larger** cosine while blue cells are **smaller**. As observed, both CLIP and BLIP have clear diagonal trends, whereas other models do not.

Another interesting observation is that the values of cosine similarity from all multimodal models are always positive, while those of combined unimodal models are either negative or positive. This holds for all datasets. Cosine similarity between any two embeddings extracted by CLIP and BLIP reduces to their dot product, which lies in the range  $[-1, 1]$ . However, due to the contrastive training objective (InfoNCE), which maximizes similarity between matched image-text pairs while merely reducing similarity among mismatched pairs, the model is not incentivized to push negative pairs to be orthogonal or negatively aligned. This leads to an embedding space that is anisotropic—where even semantically unrelated vectors often have positive cosine similarity. Prior work has observed that embeddings from contrastively trained models tend to cluster within a narrow cone in the shared



space [10, 45], leading to a high mean pairwise cosine similarity, even among unrelated samples (also happened for Meta-Transformer). This behavior reflects a bias in the learned geometry: embeddings are concentrated on a subset of directions within the high-dimensional space, rather than being isotropically distributed. This positive similarity bias implies that cosine similarity in CLIP and BLIP does not directly reflect absolute semantic distance. Rather, it is better interpreted relatively—e.g., in terms of ranking or within-batch contrast—than as a calibrated measure of dissimilarity. It is more theoretically sound for the value of cosine similarity to be in the  $[-1, 1]$  range, as similar data points should have a positive correlation while dissimilar data points should have a negative correlation.

#### 4.5. Retrieval Performance Analysis

To better understand how representation alignment may affect downstream performance, we compute Precision@K in text-to-image and image-to-text retrieval tasks. Since dataset sizes are quite different, to ensure a fair comparison, we use a random subset of 1K `<image,text>` pairs from each dataset to compute the 4 common metrics mentioned previously. Then, we use all 4K pairs from IMDB and 20K-pair subsets (for efficiency) from both Flickr30K and MS-COCO to learn the best metrics (i.e., cosine similarity) with MLPs using 2 different loss functions,<sup>5</sup> trained on random disjoint splits (80% of the data for training, 10% for validation, and 10% for testing). Considering that we use concatenated features of images and texts, the input dimensions of MLPs vary accordingly. We trained 72 MLPs in total, corresponding to 3 datasets along with 6 feature extractors in Section 4.2 for both text-to-image and image-to-text tasks, using either MSE or contrastive loss.

##### 4.5.1. Text-to-Image Retrieval

We report the results in Table 3. Regarding multimodal models, we can see that cosine similarity works best for CLIP and BLIP (both multimodal models use contrastive loss). CLIP is the best performer in IMDB, and BLIP is the best performer in Flickr30K and MS-COCO. It turns out that neither MLP with MSE nor with contrastive loss achieved good performance for learning representation similarity from multimodal models, indicating that learning similarity via a simple neural network can only approximate the

---

<sup>5</sup>Earlier experiments with different number of pairs performed similarly.



ground-truth value to a small extent. Also, when training MLPs, many stopped within 10 epochs out of 100 when using early stopping, showing the difficulty of aligning representations efficiently.

Concerning the combined unimodal models (from UM1 to UM3), all performed worse than the multimodal models, based on the 4 metrics. Again, using MLPs to learn the cosine similarity failed due to unaligned representations, and it thus demands joint training of vision and language models from scratch for a specific metric (like cosine similarity) using contrastive loss, or fine-tuning on other datasets. In this case, retrieval only performs best when we use the same metric as the one used during training, as MML models are optimized for that specific metric.

**Table 3:** Precision ( $\uparrow$ ) at  $K \in \{1, 5, 10\}$  of *text-to-image* retrieval tasks. Four commonly used metrics are directly applied to match texts with images without learning, while MLPs with either MSE or contrastive loss are used to learn the cosine similarity metric. All experiments used features extracted either by multimodal models or combined uni-modal models in Section 4.2. Best results are highlighted.

		P@1, P@5, P@10 (%)																	
Metrics		CLIP			BLIP			Meta			UM1			UM2			UM3		
IMDB	Euclidean	46.3	63.6	69.2	1.1	4.4	6.3	0.1	0.3	0.9	0.1	0.5	1.0	0.1	0.4	1.0	0.1	0.6	1.2
	Cosine	84.4	92.3	94.7	77.0	89.5	93.1	0.1	0.5	1.1	0.3	0.6	1.0	0.1	0.6	1.1	0.2	0.6	0.9
	Manhattan	78.1	90.5	92.4	0.5	3.2	5.8	0.1	0.5	1.1	0.1	0.7	1.0	0.2	0.6	1.1	0.3	0.8	1.0
	Chi-Square	0.0	0.1	0.4	0.1	0.6	1.4	0.0	0.3	1.0	0.0	0.8	1.6	0.2	0.8	1.5	0.0	0.6	0.9
	MLP (MSE)	0.5	1.0	2.0	0.7	2.0	3.7	0.3	1.7	2.7	0.3	1.2	2.7	0.0	1.0	2.7	0.3	0.5	1.7
	MLP (contr)	0.3	1.0	2.5	0.5	1.0	2.0	0.0	0.7	1.2	0.3	1.5	2.0	0.3	0.5	2.2	0.3	1.2	2.7
Flickr30K	Euclidean	16.5	45.8	57.2	0.4	5.1	10.6	0.1	0.7	1.2	0.1	0.5	1.1	0.1	0.5	1.1	0.1	0.4	0.9
	Cosine	67.2	87.9	92.4	70.6	90.7	94.3	0.0	0.6	1.2	0.1	0.5	0.7	0.2	0.4	0.7	0.1	0.5	1.0
	Manhattan	51.0	77.7	85.2	0.5	5.1	8.7	0.0	0.6	1.3	0.1	0.4	0.9	0.1	0.5	1.2	0.0	0.4	1.2
	Chi-Square	0.1	0.2	0.5	0.1	0.5	0.7	0.0	0.1	0.4	0.0	0.2	1.0	0.1	0.2	0.9	0.1	0.4	0.5
	MLP (MSE)	0.4	0.8	1.1	0.1	0.3	0.8	0.2	0.4	0.7	0.1	0.5	0.7	0.0	0.4	0.6	0.2	0.4	0.7
	MLP (contr)	0.1	0.3	0.6	0.2	0.3	0.5	0.0	0.2	0.5	0.1	0.3	0.7	0.1	0.3	0.5	0.1	0.2	0.5
MS-COCO	Euclidean	17.6	40.0	50.3	0.5	4.1	6.9	0.0	0.4	1.1	0.1	0.5	0.8	0.2	0.5	1.2	0.0	0.5	1.1
	Cosine	49.3	76.4	88.2	67.0	91.2	95.9	0.0	0.4	1.1	0.4	0.5	0.9	0.0	0.6	0.9	0.1	0.7	0.8
	Manhattan	38.8	68.7	80.1	1.0	3.7	6.1	0.0	0.4	1.4	0.1	0.5	0.8	0.0	0.5	1.1	0.1	0.6	1.1
	Chi-Square	0.2	0.5	0.9	0.1	0.6	0.9	0.0	0.1	0.6	0.1	0.3	1.1	0.0	0.2	0.7	0.1	0.8	1.1
	MLP (MSE)	0.6	2.4	4.2	0.1	0.4	0.5	0.0	0.1	0.4	0.1	0.1	0.5	0.1	0.2	0.6	0.1	0.4	0.6
	MLP (contr)	0.0	0.1	0.3	0.1	0.2	0.5	0.1	0.2	0.5	0.2	0.5	0.7	0.0	0.2	0.5	0.1	0.4	0.7

#### 4.5.2. Image-to-Text Retrieval

The results are shown in Table 4. We can see that, among all multi-modal models, CLIP outperforms BLIP for IMDB and Flickr30K datasets when using cosine similarity, while BLIP performs better than CLIP on MS-COCO for image-to-text retrieval. Both CLIP and BLIP outperform Meta-Transformer by large margins, whose performance is as worse as those of

combined unimodal models. Similar to previous analysis, the MLPs with MSE and contrastive loss performed worse than the other metrics, due to the difficulty of learning useful information from representations via MLPs. Note that retrieval results using images are not equal to those using texts (non-symmetrical), since, as shown in Figure 3, the cross-modality cosine similarity matrices are not symmetric.<sup>6</sup>

**Table 4:** Precision ( $\uparrow$ ) at  $K \in \{1, 5, 10\}$  of *image-to-text* retrieval tasks. Four commonly used metrics are directly applied to match images with texts without learning, while MLPs with either MSE or contrastive loss are used to learn the cosine similarity metric. All experiments used features extracted either by multimodal models or combined uni-modal models in Section 4.2. Best results are highlighted.

		P@1, P@5, P@10 (%)																	
Metrics		CLIP			BLIP			Meta			UM1			UM2			UM3		
IMDB	Euclidean	31.0	46.8	52.4	63.9	82.2	86.6	0.0	0.5	1.2	0.1	0.4	1.1	0.4	1.1	0.1	0.1	0.5	1.0
	Cosine	83.4	91.4	93.8	73.4	88.1	91.1	0.1	0.6	1.2	0.0	0.5	1.1	0.1	0.8	1.4	0.0	0.6	1.7
	Manhattan	79.1	89.7	92.5	49.1	71.0	78.1	0.1	0.5	0.7	0.0	0.1	0.6	0.1	0.5	1.1	0.1	0.5	1.1
	Chi-Square	0.1	0.1	0.3	0.0	0.4	1.3	0.0	0.3	0.3	0.0	0.8	1.4	0.0	0.9	1.3	0.2	0.6	1.0
	MLP (MSE)	0.5	0.7	1.7	0.0	1.5	3.4	0.3	1.2	2.5	0.3	0.7	1.5	0.5	1.7	1.7	0.3	0.5	1.7
	MLP (contr)	0.5	1.2	2.5	0.5	2.2	3.7	0.0	1.0	2.5	1.0	1.7	3.4	0.5	1.5	2.5	0.3	1.0	2.2
Flickr30K	Euclidean	48.2	63.7	68.7	47.7	79.7	88.8	0.0	0.4	1.0	0.3	0.5	1.1	0.1	0.3	1.0	0.1	0.5	1.0
	Cosine	70.1	89.1	93.3	65.3	87.9	92.8	0.0	0.4	1.0	0.2	0.5	1.2	0.1	0.6	0.8	0.1	0.6	1.5
	Manhattan	60.8	81.9	87.3	40.2	70.8	81.7	0.0	0.5	0.8	0.1	0.5	1.2	0.1	0.5	0.9	0.1	0.4	1.1
	Chi-Square	0.0	0.1	0.4	0.1	0.3	0.6	0.0	0.3	0.4	0.0	0.4	1.2	0.0	0.4	0.9	0.0	0.2	0.7
	MLP (MSE)	0.1	0.8	1.4	0.2	0.3	0.7	0.0	0.2	0.5	0.0	0.1	0.2	0.1	0.4	0.6	0.1	0.3	0.6
	MLP (contr)	0.1	0.4	0.7	0.0	0.2	0.3	0.1	0.3	0.6	0.1	0.3	0.7	0.0	0.4	0.7	0.1	0.3	0.6
MS-COCO	Euclidean	32.2	55.0	65.2	48.0	82.5	93.4	0.2	0.4	0.9	0.0	0.2	0.5	0.1	0.5	1.1	0.1	0.5	0.9
	Cosine	51.0	82.3	92.2	64.7	90.1	96.0	0.1	0.3	0.7	0.0	0.2	0.7	0.0	0.3	0.6	0.1	0.6	1.2
	Manhattan	43.4	73.5	86.1	42.0	74.9	86.7	0.0	0.5	1.1	0.0	0.3	0.7	0.0	0.7	1.4	0.1	0.5	1.0
	Chi-Square	0.0	0.4	1.0	0.0	0.6	1.0	0.1	0.5	1.0	0.1	0.3	0.9	0.0	0.3	0.8	0.1	0.5	1.3
	MLP (MSE)	0.2	0.7	1.7	0.1	0.2	0.4	0.0	0.3	0.5	0.1	0.1	0.4	0.2	0.4	0.4	0.1	0.2	0.4
	MLP (contr)	0.2	0.5	0.7	0.2	0.3	0.5	0.1	0.3	0.5	0.1	0.1	0.3	0.1	0.4	0.6	0.1	0.2	0.5

No matter if it is image-to-text or text-to-image, cosine similarity performs best for CLIP and BLIP, which is unsurprising due to the contrastive loss being part of (or the whole) objective function. As shown in Table 3 and Table 4, CLIP outperforms in image-to-text tasks, achieving the best results on 2 out of 3 datasets. In contrast, BLIP performs better in text-to-image tasks, also winning on 2 out of 3 datasets, despite having the smallest modality described in Section 4.3. Notably, BLIP consistently outperforms CLIP on MS-COCO. These results highlight the significant variability in model perfor-

<sup>6</sup>In our experiments, given an embedding in one modality, we compute the cosine similarity against *all* embeddings in the other modality, and vice versa.

mance across different datasets. Moreover, cosine similarity cannot perform equally good for both tasks since the mean of cosine similarity across images with respect to all texts is not equal to the mean of cosine similarity across texts with respect to all images. As for Euclidean and Manhattan distances, they perform better for image-to-text than text-to-image tasks when using CLIP and BLIP, which might be coincidental as they are measuring different geometric aspects and are not part of their objective functions.

Now we use all captions from the test split (1K) of Flickr30K to inspect the performance of CLIP and BLIP models based on cosine similarity. The results are shown in Table 5. For image-to-text retrieval tasks using models, we observe a decline in precision as the retrieval scope widens (e.g., from  $P@1$  to  $P@10$ ). This phenomenon arises because, in these experiments, each image can have up to five ground-truth captions. For text-to-image tasks, where each caption corresponds to one image, the upper bounds differ significantly. For both retrieval tasks, the upper-bound precision values are constrained by the dataset structure (five captions per image). See Appendix A for more details.

**Table 5:** Precision for retrieval tasks using CLIP and BLIP models on the 1K test split of Flickr30K with 5 captions.

	Image-to-text			Text-to-image		
	P@1	P@5	P@10	P@1	P@5	P@10
<b>CLIP</b>	79.30	58.06	36.27	58.92	16.69	9.01
<b>BLIP</b>	66.00	53.12	34.47	61.44	16.82	8.95

For both image-to-text and text-to-image retrieval tasks, MLPs failed to learn the cosine similarity between image and text features, regardless of the loss function used, indicating the huge gap between theory and practice. One reason is that the MLP architecture is overly simplistic and cannot hold infinite neurons due to hardware constraints, although it is the most appropriate choice for this task. Furthermore, we found bottleneck layers in Optuna-searched MLPs (i.e., an MLP with 3 hidden layers having 700-100-700 neurons), which suggests potential learning problems. To verify this assumption, we manually re-designed the MLP architecture to have down-projections of 500-300-100 neurons (see Table 6), and observed worse performance in most cases. Another reason may be that cosine similarity cannot be learned as intended, as any small difference between the learned and the true

cosine similarity might produce significantly different rankings, thus affecting retrieval performance and thereby calling for more sophisticated methods in the future.

**Table 6:** Precision ( $\uparrow$ ) at  $K \in \{1, 5, 10\}$  for down-projection MLPs having 500-300-100 hidden neurons with MSE loss in text-to-image retrieval tasks. Better or worse results than those obtained via Optuna-searched MLPs in Table 3 are highlighted. Similar results were observed for image-to-text retrieval tasks.

	IMDB			Flickr30K			MS-COCO		
<b>CLIP</b>	0.5	2.0	3.0	0.1	0.4	0.7	0.2	0.8	1.6
<b>BLIP</b>	0.7	1.7	2.5	0.1	0.5	0.7	0.1	0.2	0.4

To conclude these experiments, we conducted statistical tests to corroborate the significance of our results. Pairwise comparisons (Bonferroni-Holm corrected) using the Chi-square test of proportions revealed statistically significant differences between CLIP and BLIP and all the other models, in all datasets, both in image-to-text and text-to-image retrieval experiments, for all top-K results and Euclidean, Cosine, and Manhattan metrics ( $p < .0001$ ). No statistically significant differences were found between Meta-transformer, UM1, UM2, and UM3, for any of the top-K results and any of the metrics ( $p > .05$ ) in any dataset or retrieval task.

#### 4.5.3. Sample Outputs

Here we provide real-world application examples using feature representations from CLIP to retrieve images given some texts and vice versa. The leftmost column depicts the input query (either images or texts), and the other columns show the top-5 retrieved results.

In Figure 4, CLIP retrieved the right poster image for the given title as the top-1 result on IMDB. It also correctly retrieved the right scenario as the top-1 result on Flickr30k. The top-4 result was retrieved for MS-COCO as well, although the dataset covers a wide range of complex and diverse scenarios. From the examples, it might be surprising that CLIP performs so well on the IMDB dataset, since movie names are rather short and often not semantically related to their poster images. This might be the result of potential overlap between the training data of CLIP and the IMDB dataset, as well as CLIP’s excellent zero-shot performance. On the other hand, MS-COCO has more diverse images that cover more scenarios and is thus proved

more challenging for retrieval tasks, which underscores the lower performance compared to IMDB and Flickr30k, as in Table 3 and Table 4.

Figure 5 shows the retrieval results of text descriptions when given images as input. CLIP successfully retrieved corresponding descriptions within top-5 results for IMDB and Flickr30K, whereas it failed on MS-COCO. From multiple rounds of retrieval results, we found that CLIP’s language understanding capability is not symmetric to its visual understanding on certain cases, which could be a result of an asymmetric contrastive loss and different understanding capabilities of visual and language encoders. Our retrieval results corroborate the aforementioned analysis.

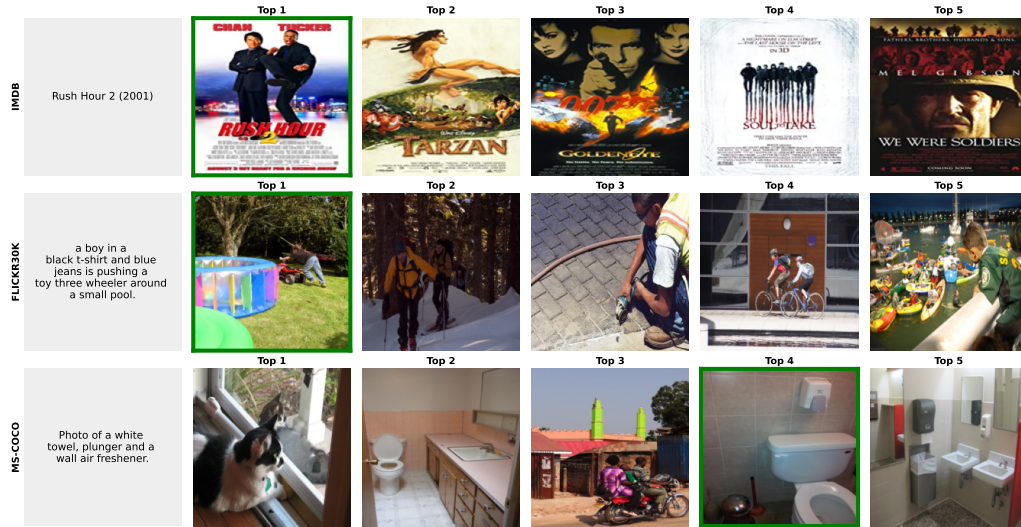


**Figure 4:** Image retrieval examples given randomly selected texts as input queries using CLIP. Correct results marked in green. CLIP successfully retrieved the corresponding image on all datasets, although for MS-COCO it was at position 4.

The examples of retrieval results for BLIP and Meta-Transformers are shown in Appendix B. We noted that Meta-Transformer performed significantly worse than BLIP and CLIP models, as informed by the results of the experiments presented in Section 4.4 section, even though Meta-Transformer’s modality gap is close to these of CLIP and BLIP.

## 5. Discussion, Limitations, and Future Work

Our experiments systematically assess the extent to which learned features from multimodal and combined unimodal models can be leveraged in

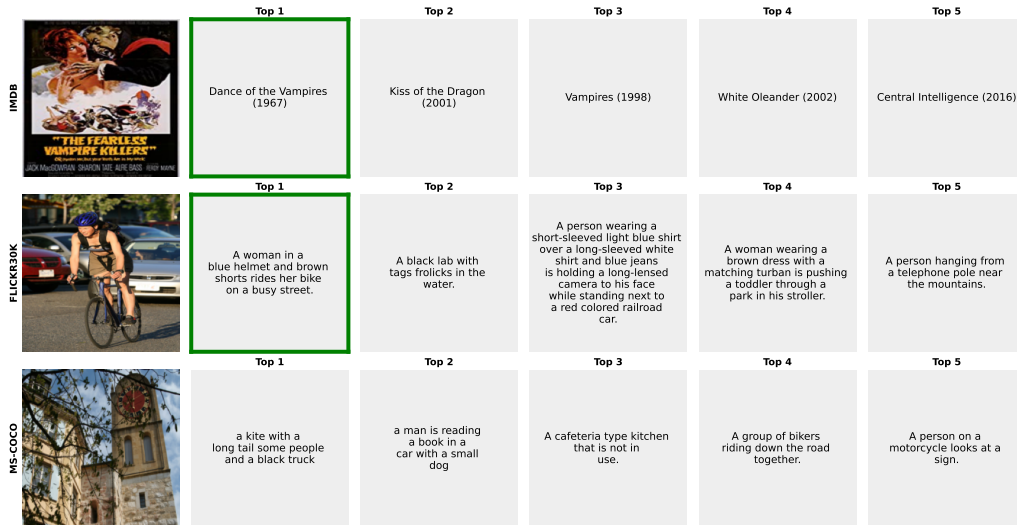


**Figure 5:** Text retrieval examples given randomly selected images as input queries using CLIP. **Correct results** marked in green. CLIP successfully retrieved the corresponding text on IMDB and Flickr30K datasets, whereas it failed on MS-COCO.

cross-modality retrieval tasks. To the best of our knowledge, this is the first work to investigate this complex and underexplored direction. The key insights from our experiments are:

- The geometry of multimodal representations does not necessarily correlate with retrieval performance.
- When both textual and visual embeddings are obtained from the same multimodal model, cosine similarity consistently outperforms alternative similarity metrics.
- Training MLPs to learn separate textual and visual representations proves inefficient, whereas jointly training unimodal models yields better performance.

We now outline the key limitations and open questions emerging from our findings, to motivate future research directions.

First of all, and perhaps not surprisingly, our experiments show that there is no single model that consistently outperforms others in all tasks and datasets. For example, CLIP outperforms BLIP on the IMDB dataset for

both text-to-image and image-to-text retrieval tasks, whereas BLIP outperforms CLIP on the MS-COCO dataset for the same tasks.

Distribution shifts are an inherent aspect of machine learning systems. Applying t-SNE to visualize features extracted from different layers of a neural network may yield varying results. This variability arises due to evolving feature representations across network layers, which can lead to changes in the underlying data distribution [65]. When the input distribution to t-SNE is altered, the resulting low-dimensional embeddings reflect the distribution of the transformed features, rather than the original data distribution. Consequently, dimensionality reduction techniques such as t-SNE primarily reveal feature-space structures induced by the model, rather than faithfully representing the intrinsic structure of the raw data.

Mathematically anomalous similarity values may arise in practice. As illustrated in Figure 3, cosine similarity scores derived from multimodal models are consistently positive, whereas those from unimodal models can take both positive and negative values. Theoretically, a positive cosine similarity indicates that a textual and visual feature pair is semantically similar, while a negative value suggests dissimilarity. Therefore, an effective metric for evaluating feature alignment should not only capture the degree of similarity but also meaningfully reflect dissimilarity. Ideally, such a metric would produce a weighted score that accounts for both aspects. For instance, the cosine similarity between the feature representation of an image depicting a human face and that of the word “banana” should yield a negative value, reflecting their substantial semantic divergence. A small positive score in such a case would misrepresent the true nature of their relationship, underestimating the extent of their dissimilarity.

Our experiments reveal an inverse relationship between dataset diversity and retrieval precision. Specifically, models achieve higher precision on less diverse datasets (e.g., IMDB) compared to more diverse collections (e.g., MS-COCO). This performance degradation stems from increased out-of-distribution samples in diverse datasets, which challenge model robustness [66].

Computational scalability presents another significant constraint: Cross-modal similarity computation scales quadratically,  $\mathcal{O}(N^2)$  with dataset cardinality  $N$  under one-to-one modality mapping assumptions. This complexity imposes practical limitations on large-scale retrieval systems.

Current image encoders exhibit limited capability in capturing fine-grained visual details, deterring precise image-text alignment. We emphasize however



that, as mentioned in [Section 4.1](#), this limitation is unrelated to image resizing, as evidenced by SPARC [62] which achieves fine-detail understanding on  $224 \times 224$  pixel inputs through contrastive language-visual alignment. While models like the one presented by Iscen et al. [67] demonstrate promising cross-modal refinement, their restricted availability hinders practical adoption.

On the other hand, text encoders face two main limitations: (1) Input truncation (e.g., 76 tokens in CLIP, 512 in BLIP) constrains comprehension of lengthy documents, potentially addressable through LLM-based summarization preprocessing; (2) Performance degradation on non-English texts due to English-centric training, exacerbating challenges for low-resource languages [68]. Effective multilingual support necessitates comprehensive training data in target languages to capture language-specific semantic nuances.

Finally, we observed a geometric constraint in multimodal embedding spaces: representations typically occupy a narrow cone—a phenomenon exacerbated by contrastive learning objectives. This induces a modality gap where representations become linearly separable but hinder MLP-based fusion approaches, as demonstrated in our experiments. This fundamental limitation of combined unimodal models warrants novel geometric alignment techniques in future multimodal architectures.

## 6. Conclusion

This work systematically examines the alignment of visual and textual representations through both VLMs and integrated unimodal architectures, employing four established metrics alongside two learned ones. Our analysis demonstrates that embedding space alignment can be effectively quantified through distributional distance metrics. Crucially, we observe that multimodal models trained with contrastive loss, despite inducing a modality gap, consistently outperform integrated unimodal counterparts when evaluated using cosine similarity. Furthermore, we establish that simplistic architectural approaches, such as MLPs, prove insufficient for modeling the complex cross-modal interactions between representations. Collectively, these findings provide substantive new research perspectives for cross-modal information retrieval utilizing MML frameworks. To facilitate reproducibility and further investigation, our implementation will be made publicly available upon publication.



## Acknowledgments

We thank Niculae Sebe and Fabrizio Silvestri for reviewing an earlier version of this paper. The authors gratefully acknowledge Luxembourg’s national supercomputer MeluXina and the LuxProvide teams for their expert support. This research is supported by the D4H PRIDE DTU, funded by Luxembourg’s Fonds National de la Recherche (FNR), and Horizon Europe’s European Innovation Council through the Pathfinder program (SYM-BIOTIK, grant 101071147).

## References

- [1] Y. LeCun, B. Boser, J. S. Denker, D. Henderson, R. E. Howard, W. Hubbard, L. D. Jackel, Backpropagation applied to handwritten zip code recognition, *Neural Computation* (1989).
- [2] A. Vaswani, N. Shazeer, N. Parmar, J. Uszkoreit, L. Jones, A. N. Gomez, L. u. Kaiser, I. Polosukhin, Attention is all you need, in: *Advances in Neural Information Processing Systems (NeurIPS)*, Curran Associates, Inc., 2017.
- [3] A. Dosovitskiy, L. Beyer, A. Kolesnikov, D. Weissenborn, X. Zhai, T. Unterthiner, M. Dehghani, M. Minderer, G. Heigold, S. Gelly, J. Uszkoreit, N. Houlsby, An image is worth 16x16 words: Transformers for image recognition at scale, in: *9th International Conference on Learning Representations (ICLR)*, 2021.
- [4] J. Devlin, M.-W. Chang, K. Lee, K. Toutanova, BERT: Pre-training of deep bidirectional transformers for language understanding, in: *Proceedings of the 2019 Conference of the North American Chapter of the Association for Computational Linguistics: Human Language Technologies (NAACL)*, 2019.
- [5] A. Radford, K. Narasimhan, T. Salimans, I. Sutskever, Improving language understanding by generative pre-training, 2018. [https://cdn.openai.com/research-covers/language-unsupervised/language\\_understanding\\_paper.pdf](https://cdn.openai.com/research-covers/language-unsupervised/language_understanding_paper.pdf).
- [6] A. Radford, J. Wu, R. Child, D. Luan, D. Amodei, I. Sutskever, Language models are unsupervised multitask learners, *OpenAI*

- (2019). URL: [https://cdn.openai.com/better-language-models/language\\_models\\_are\\_unsupervised\\_multitask\\_learners.pdf](https://cdn.openai.com/better-language-models/language_models_are_unsupervised_multitask_learners.pdf).
- [7] T. B. Brown, B. Mann, N. Ryder, M. Subbiah, J. Kaplan, P. Dhariwal, A. Neelakantan, P. Shyam, G. Sastry, A. Askell, S. Agarwal, A. Herbert-Voss, G. Krueger, T. Henighan, R. Child, A. Ramesh, D. M. Ziegler, J. Wu, C. Winter, C. Hesse, M. Chen, E. Sigler, M. Litwin, S. Gray, B. Chess, J. Clark, C. Berner, S. McCandlish, A. Radford, I. Sutskever, D. Amodei, Language models are few-shot learners, in: Proceedings of the 34th International Conference on Neural Information Processing Systems (NeurIPS), 2020.
  - [8] A. Radford, J. W. Kim, C. Hallacy, A. Ramesh, G. Goh, S. Agarwal, G. Sastry, A. Askell, P. Mishkin, J. Clark, G. Krueger, I. Sutskever, Learning transferable visual models from natural language supervision, in: Proceedings of the 38th International Conference on Machine Learning (ICML), Proceedings of Machine Learning Research, PMLR, 2021.
  - [9] J. Li, D. Li, C. Xiong, S. Hoi, BLIP: Bootstrapping language-image pre-training for unified vision-language understanding and generation, in: Proceedings of the 39th International Conference on Machine Learning (ICML), Proceedings of Machine Learning Research, PMLR, 2022.
  - [10] V. W. Liang, Y. Zhang, Y. Kwon, S. Yeung, J. Y. Zou, Mind the gap: Understanding the modality gap in multi-modal contrastive representation learning, in: Advances in Neural Information Processing Systems (NeurIPS), 2022.
  - [11] K. Hornik, Approximation capabilities of multilayer feedforward networks, Neural Networks (1991). doi:[https://doi.org/10.1016/0893-6080\(91\)90009-T](https://doi.org/10.1016/0893-6080(91)90009-T).
  - [12] Z. Li, F. Liu, W. Yang, S. Peng, J. Zhou, A survey of convolutional neural networks: Analysis, applications, and prospects, IEEE Transactions on Neural Networks and Learning Systems (2022).
  - [13] K. He, X. Zhang, S. Ren, J. Sun, Deep residual learning for image recognition, in: 2016 IEEE Conference on Computer Vision and Pattern Recognition (CVPR), 2016.

- [14] S. d’Ascoli, H. Touvron, M. L. Leavitt, A. S. Morcos, G. Biroli, L. Sagun, ConViT: improving vision transformers with soft convolutional inductive biases, *Journal of Statistical Mechanics: Theory and Experiment* (2022).
- [15] Y. Li, H. Mao, R. Girshick, K. He, Exploring plain vision transformer backbones for object detection, in: *European conference on computer vision (ECCV)*, Springer, 2022, pp. 280–296.
- [16] Z. Liu, H. Mao, C.-Y. Wu, C. Feichtenhofer, T. Darrell, S. Xie, A convnet for the 2020s, in: *Proceedings of the IEEE/CVF conference on computer vision and pattern recognition (CVPR)*, 2022, pp. 11976–11986.
- [17] Z. Liu, Y. Lin, Y. Cao, H. Hu, Y. Wei, Z. Zhang, S. Lin, B. Guo, Swin transformer: Hierarchical vision transformer using shifted windows, in: *Proceedings of the IEEE/CVF international conference on computer vision (ICCV)*, 2021.
- [18] Y. Liu, M. Ott, N. Goyal, J. Du, M. Joshi, D. Chen, O. Levy, M. Lewis, L. Zettlemoyer, V. Stoyanov, Roberta: A robustly optimized BERT pretraining approach, *CoRR arXiv: abs/1907.11692* (2019).
- [19] P. He, X. Liu, J. Gao, W. Chen, Deberta: Decoding-enhanced bert with disentangled attention, *CoRR arXiv: abs/2006.03654* (2020).
- [20] Z. Yang, Z. Dai, Y. Yang, J. Carbonell, R. R. Salakhutdinov, Q. V. Le, Xlnet: Generalized autoregressive pretraining for language understanding, in: *Advances in Neural Information Processing Systems (NeurIPS)*, volume 32, Curran Associates, Inc., 2019.
- [21] H. Touvron, T. Lavril, G. Izacard, X. Martinet, M.-A. Lachaux, T. Lacroix, B. Rozière, N. Goyal, E. Hambro, F. Azhar, A. Rodriguez, A. Joulin, E. Grave, G. Lample, LLaMA: Open and efficient foundation language models, *CoRR ArXiv:abs/2302.13971* (2023).
- [22] BigScience Workshop, BLOOM: A 176b-parameter open-access multilingual language model, 2023.
- [23] Z. Du, Y. Qian, X. Liu, M. Ding, J. Qiu, Z. Yang, J. Tang, GLM: General language model pretraining with autoregressive blank infilling, in:

Proceedings of the 60th Annual Meeting of the Association for Computational Linguistics (ACL), 2022.

- [24] J. Li, D. Li, S. Savarese, S. Hoi, BLIP-2: Bootstrapping language-image pre-training with frozen image encoders and large language models, in: Proceedings of the 40th International Conference on Machine Learning (ICML), Proceedings of Machine Learning Research, PMLR, 2023.
- [25] Y. Zhang, K. Gong, K. Zhang, H. Li, Y. Qiao, W. Ouyang, X. Yue, Meta-transformer: A unified framework for multimodal learning, CoRR arXiv:abs/2307.10802 (2023).
- [26] Z. Tang, Z. Yang, C. Zhu, M. Zeng, M. Bansal, Any-to-any generation via composable diffusion, in: Advances in Neural Information Processing Systems (NeurIPS), 2024.
- [27] J.-B. Alayrac, J. Donahue, P. Luc, A. Miech, I. Barr, Y. Hasson, K. Lenc, A. Mensch, K. Millican, M. Reynolds, et al., Flamingo: a visual language model for few-shot learning, in: Proceedings of the 36th International Conference on Advances in neural information processing systems (NeurIPS), volume 35, 2022, pp. 23716–23736.
- [28] L. Yuan, D. Chen, Y.-L. Chen, N. Codella, X. Dai, J. Gao, H. Hu, X. Huang, B. Li, C. Li, et al., Florence: A new foundation model for computer vision, CoRR arXiv:abs/2111.11432 (2021).
- [29] B. Xiao, H. Wu, W. Xu, X. Dai, H. Hu, Y. Lu, M. Zeng, C. Liu, L. Yuan, Florence-2: Advancing a unified representation for a variety of vision tasks, in: Proceedings of the IEEE/CVF Conference on Computer Vision and Pattern Recognition (CVPR), 2024.
- [30] C. Wu, S. Yin, W. Qi, X. Wang, Z. Tang, N. Duan, Visual chatgpt: Talking, drawing and editing with visual foundation models, CoRR arXiv:abs/2303.04671 (2023).
- [31] W. Wang, Q. Lv, W. Yu, W. Hong, J. Qi, Y. Wang, J. Ji, Z. Yang, L. Zhao, X. Song, et al., Cogvlm: Visual expert for pretrained language models, CoRR arXiv:abs/2311.03079 (2023).

- [32] F. Chen, M. Han, H. Zhao, Q. Zhang, J. Shi, S. Xu, B. Xu, X-llm: Bootstrapping advanced large language models by treating multi-modalities as foreign languages, CoRR arXiv:abs/2305.04160 (2023).
- [33] L. H. Li, M. Yatskar, D. Yin, C.-J. Hsieh, K.-W. Chang, Visualbert: A simple and performant baseline for vision and language, CoRR arXiv:abs/1908.03557 (2019).
- [34] D. Zhang, S. Li, X. Zhang, J. Zhan, P. Wang, Y. Zhou, X. Qiu, SpeechGPT: Empowering large language models with intrinsic cross-modal conversational abilities, in: Findings of the Association for Computational Linguistics (EMNLP), Association for Computational Linguistics, 2023.
- [35] S. Wu, H. Fei, L. Qu, W. Ji, T.-S. Chua, Next-gpt: Any-to-any multi-modal llm, CoRR arXiv:abs/2309.05519 (2023).
- [36] Z. Li, X. Wu, H. Du, F. Liu, H. Nghiem, G. Shi, A survey of state of the art large vision language models: Alignment, benchmark, evaluations and challenges, CoRR ArXiv (2025). [arXiv:abs/2501.02189](https://arxiv.org/abs/2501.02189).
- [37] R. Hadsell, S. Chopra, Y. LeCun, Dimensionality reduction by learning an invariant mapping, in: Proceedings of the IEEE/CVF conference on computer vision and pattern recognition (CVPR), 2006.
- [38] A. van den Oord, Y. Li, O. Vinyals, Representation learning with contrastive predictive coding, CoRR abs/1807.03748 (2018).
- [39] K. He, H. Fan, Y. Wu, S. Xie, R. Girshick, Momentum contrast for unsupervised visual representation learning, in: IEEE/CVF Conference on Computer Vision and Pattern Recognition (CVPR), 2020.
- [40] T. Chen, S. Kornblith, M. Norouzi, G. Hinton, A simple framework for contrastive learning of visual representations, in: Proceedings of the 37th International Conference on Machine Learning (ICML), Proceedings of Machine Learning Research, 2020.
- [41] J.-B. Grill, F. Strub, F. Altché, C. Tallec, P. Richemond, E. Buchatskaya, C. Doersch, B. Avila Pires, Z. Guo, M. Gheshlaghi Azar,

- B. Piot, k. kavukcuoglu, R. Munos, M. Valko, Bootstrap your own latent - a new approach to self-supervised learning, in: Advances in Neural Information Processing Systems (NeurIPS), 2020.
- [42] C. Jia, Y. Yang, Y. Xia, Y.-T. Chen, Z. Parekh, H. Pham, Q. Le, Y.-H. Sung, Z. Li, T. Duerig, Scaling up visual and vision-language representation learning with noisy text supervision, in: Proceedings of the 38th International Conference on Machine Learning (ICML), Proceedings of Machine Learning Research, 2021.
- [43] X. Zhai, B. Mustafa, A. Kolesnikov, L. Beyer, Sigmoid loss for language image pre-training, in: Proceedings of the IEEE/CVF international conference on computer vision (ICCV), 2023.
- [44] B. A. Yilma, L. A. Leiva, Together yet apart: Multimodal representation learning for personalised visual art recommendation, in: Proceedings of the ACM Conf. on User Modeling, Adaptation and Personalization (UMAP), 2023.
- [45] K. Ethayarajh, How contextual are contextualized word representations? Comparing the geometry of BERT, ELMo, and GPT-2 embeddings, in: Proceedings of the 2019 Conference on Empirical Methods in Natural Language Processing and the 9th International Joint Conference on Natural Language Processing (EMNLP-IJCNLP), 2019. doi:[10.18653/v1/D19-1006](https://doi.org/10.18653/v1/D19-1006).
- [46] W. Wang, X. Yang, B. C. Ooi, D. Zhang, Y. Zhuang, Effective deep learning-based multi-modal retrieval, The VLDB Journal (2016).
- [47] J. Luo, Y. Shen, X. Ao, Z. Zhao, M. Yang, Cross-modal image-text retrieval with multitask learning, in: Proceedings of the 28th ACM International Conference on Information and Knowledge Management (CIKM), Association for Computing Machinery, 2019.
- [48] L. Zhen, P. Hu, X. Peng, R. S. M. Goh, J. T. Zhou, Deep multimodal transfer learning for cross-modal retrieval, IEEE Transactions on Neural Networks and Learning Systems (2022).
- [49] K. Kumar, T. Arici, T. Neiman, J. Yang, S. Sam, Y. Xu, H. Ferhatosmanoglu, I. Tutar, Unsupervised multi-modal representation learning

- for high quality retrieval of similar products at e-commerce scale, in: Proceedings of the 32nd ACM International Conference on Information and Knowledge Management (CIKM), 2023.
- [50] G. Luo, L. Dunlap, D. H. Park, A. Holynski, T. Darrell, Diffusion hyperfeatures: Searching through time and space for semantic correspondence, in: Advances in Neural Information Processing Systems (NeurIPS), Curran Associates, Inc., 2023.
  - [51] L. V. B. Beltrán, J. C. Caicedo, N. Journet, M. Coustaty, F. Lecellier, A. Doucet, Deep multimodal learning for cross-modal retrieval: One model for all tasks, Pattern Recognition Letters (2021).
  - [52] T. Yu, Y. Yang, H. Fei, Y. Li, X. Chen, P. Li, Assorted attention network for cross-lingual language-to-vision retrieval, in: Proceedings of the 30th ACM International Conference on Information & Knowledge Management (CIKM), Association for Computing Machinery, 2021.
  - [53] L. van der Maaten, G. Hinton, Visualizing data using t-SNE, Journal of Machine Learning Research (2008).
  - [54] L. McInnes, J. Healy, N. Saul, L. Großberger, Umap: Uniform manifold approximation and projection, Journal of Open Source Software 3 (2018) 861.
  - [55] S. Zhu, L. Liu, Y. Wang, Information retrieval using hellinger distance and sqrt-cos similarity, in: 2012 7th International Conference on Computer Science & Education (ICCSE), 2012.
  - [56] B. Acree, E. Hansen, J. Jansa, K. Shoub, Comparing and evaluating cosine similarity scores, weighted cosine similarity scores and substring matching, Working Paper (2016).
  - [57] S. Tan, Z. Zhou, Z. Xu, P. Li, On efficient retrieval of top similarity vectors, in: Proceedings of the 2019 Conference on Empirical Methods in Natural Language Processing and the 9th International Joint Conference on Natural Language Processing (EMNLP-IJCNLP), Association for Computational Linguistics, 2019.

- [58] H. Gong, T. Sakakini, S. Bhat, J. Xiong, Document similarity for texts of varying lengths via hidden topics, in: Proceedings of the 56th Annual Meeting of the Association for Computational Linguistics (ACL), 2018.
- [59] X. Zhang, IMDB Vision and NLP, 2022. doi:[10.34740/KAGGLE/DS/1937446](https://doi.org/10.34740/KAGGLE/DS/1937446).
- [60] P. Young, A. Lai, M. Hodosh, J. Hockenmaier, From image descriptions to visual denotations: New similarity metrics for semantic inference over event descriptions, Transactions of the Association for Computational Linguistics (ACL) (2014).
- [61] T.-Y. Lin, M. Maire, S. Belongie, J. Hays, P. Perona, D. Ramanan, P. Dollár, C. L. Zitnick, Microsoft coco: Common objects in context, in: The 13th European Conference on Computer Vision (ECCV), Springer, 2014.
- [62] I. Bica, A. Ilic, M. Bauer, G. Erdogan, M. Bošnjak, C. Kaplanis, A. A. Gritsenko, M. Minderer, C. Blundell, R. Pascanu, J. Mitrovic, Improving fine-grained understanding in image-text pre-training, in: R. Salakhutdinov, Z. Kolter, K. Heller, A. Weller, N. Oliver, J. Scarlett, F. Berkenkamp (Eds.), Proceedings of the 41st International Conference on Machine Learning (ICML), Proceedings of Machine Learning Research, PMLR, 2024.
- [63] I. T. Jolliffe, J. Cadima, Principal component analysis: a review and recent developments, Philosophical Transactions of the Royal Society A: Mathematical, Physical and Engineering Sciences (2016).
- [64] M. Hearst, S. Dumais, E. Osuna, J. Platt, B. Scholkopf, Support vector machines, IEEE Intelligent Systems and their Applications (1998).
- [65] O. Wiles, S. Goyal, F. Stimberg, S.-A. Rebuffi, I. Ktena, K. D. Dvijotham, A. T. Cemgil, A fine-grained analysis on distribution shift, in: International Conference on Learning Representations (ICLR), 2022.
- [66] A. Robey, H. Hassani, G. J. Pappas, Model-based robust deep learning, CoRR arXiv:abs/2005.10247 (2020).
- [67] A. Iscen, M. Caron, A. Fathi, C. Schmid, Retrieval-enhanced contrastive vision-text models, CoRR arXiv:abs/2306.07196 (2023).



- [68] C. Wendler, V. Veselovsky, G. Monea, R. West, Do llamas work in English? on the latent language of multilingual transformers, in: Proceedings of the 62nd Annual Meeting of the Association for Computational Linguistics (ACL), Association for Computational Linguistics, 2024.

## Appendix A. Precision for images with 5 captions from Flickr30K

Figure A.1 shows the upper bounds for retrieval Precision at different ranking sizes  $K$ . As  $K$  increases, the denominator grows faster than the numerator. While five captions per image increase the pool of potentially relevant matches, this advantage diminishes when  $K > 5$ , as the fixed number of ground-truth captions cannot offset the quadratic growth of retrieved samples. Here, Precision drops more sharply because the single relevant image per caption cannot compensate for the rapidly growing denominator. This asymmetry highlights how dataset design (multiple captions per image vs. single-image matches) fundamentally impacts P@K trends in cross-modal retrieval. Notably, at  $K = 5$ , image-to-text retrieval maintains perfect Precision (1.0) while text-to-image precision collapses to 0.2, demonstrating the critical role of annotation multiplicity in retrieval effectiveness.

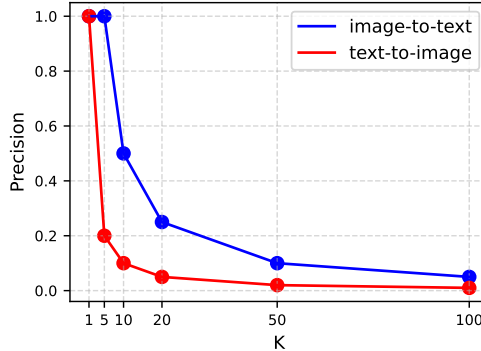


**Figure A.1:** Upper bounds of P@K on the test split of Flickr30K. The drop is more significant for text-to-images retrieval tasks, as each annotation only corresponds to one image, whereas each image matches five annotations for image-to-text retrieval instead.

## Appendix B. BLIP and Meta-Transformer Retrieval Examples

We show more retrieval examples on text-to-image and image-to-text tasks using BLIP model in Figure B.1 and Figure B.2. From both of the

figures, we observe a good retrieval performance on all 3 datasets when using BLIP model.



**Figure B.1:** Image retrieval examples given randomly selected texts as input queries using BLIP on three datasets. Correct results are marked in green. BLIP successfully retrieves corresponding images on all datasets.

Features extracted by Meta-Transformer performs poorly when used to match texts with images, as no results is correctly retrieved. Results are shown in Figure B.3 and Figure B.4, from which we barely observe connections between input queries and outputs.



**Figure B.2:** Text retrieval examples given randomly selected images as input queries using BLIP on three datasets. Correct results are marked in **green**. BLIP successfully retrieves corresponding texts on all datasets.



**Figure B.3:** Image retrieval examples given randomly selected texts as input queries using Meta-Transformer on three datasets. No correct results are retrieved in these cases.

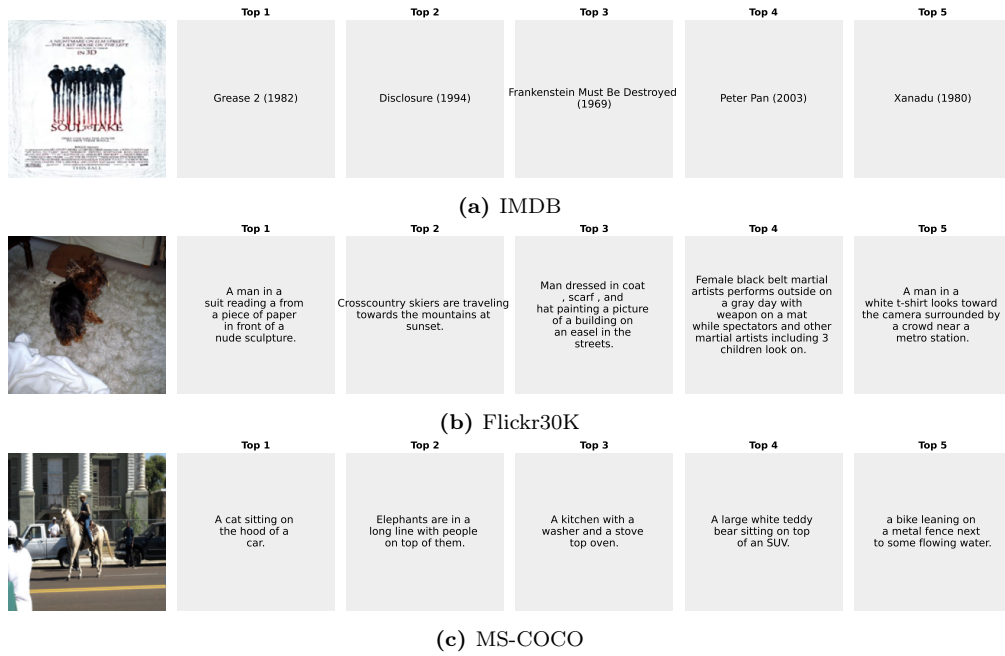


**Figure B.4:** Text retrieval examples given randomly selected images as input queries using Meta-Transformer on three datasets. No correct results are retrieved in these cases.